Aerospace Science and Technology, 1999, no. 5, 261–270

Two-dimensional wake vortex physics in the stably stratified atmosphere

F. Holzäpfel *, T. Gerz

Institut für Physik der Atmosphäre, DLR Oberpfaffenhofen, 82234 Weßling, Germany

(Received 15 February1999, revised and accepted 12 May 1999)

Holzäpfel F., Gerz T., *Aerospace Science and Technology*, 1999, no. 5, 261–270

Abstract

The effects of stable stratification on aircraft wake vortices are investigated by means of high-resolution two-dimensional simulations. The simulations elucidate that the vortices first decelerate and then accelerate their descent, where they largely conserve their circulation. However, for very stable stratification the tip vortices may rise again to the flight path. The underlying physical mechanisms are revealed by means of a point vortex method and are examined complementarily by balancing the impulse of the wake vortices. It is shown that the prominant effects, deceleration, detrainment and acceleration, are caused by the kinematic interaction of the vorticity generated by baroclinity and the primary vorticity. Furthermore, it is found that the impulse of the 'whole' system, including the detrained secondary vorticity, is oscillating with the Brunt-Väisälä frequency which implies that the wingtip vortices themselves do not. Finally, a local shear-number is proposed which takes into account the interaction of primary and secondary vorticity and can describe the instantaneous tendency of wake vortices to accelerate or to decelerate. © Elsevier, Paris

wake vortex / stable stratification / numerical simulation

Zusammenfassung

Zur Physik der Wirbelschleppe in der stabil geschichteten Atmosphäre. Der Einfluß stabil geschichteter Atmosphäre auf die Entwicklung von Flugzeug-Wirbelschleppen wird mittels hochauflösender, zweidimensionaler Simulationen untersucht. Zunächst sinken die Wirbel verzögert und in einer späteren Phase beschleunigt ab. Dabei wird die Zirkulation der Wirbel weitgehend erhalten. Jedoch steigen die Wirbel in einer sehr stabil geschichteten Umgebung wieder bis auf Flugniveau auf. Die zugrundeliegende Physik der beobachteten Effekte wird mit Hilfe einer Punktwirbelmethode und anhand von Impulsbilanzen untersucht. Es wird gezeigt, daß die wichtigsten Phänomene, die Verzögerung, das Detrainment und die Beschleunigung der Wirbel, durch die kinematische Wechselwirkung primärer und baroklin erzeugter Vorticity verursacht werden. Weiterhin wird gezeigt, daß der Impuls des gesamten Wirbelsystems, einschließlich der detrainten Vorticity, mit der Brunt-Väisälä Frequenz oszilliert, während die eigentliche Wirbelschleppe dies nicht tut. Schließlich wird eine lokale Scherzahl abgeleitet, die die momentane Neigung der Wirbelschleppe verzögert oder beschleunigt abzusinken beschreibt. © Elsevier, Paris

Wirbelschleppe / stabile Schichtung / numerische Simulation

* Correspondence and reprints.

1. Introduction

Aircraft wake vortices may exert a serious danger on following aircraft if the separation between leading and following aircraft is not sufficient. In view of the expected growth of air traffic [29], increasing demands on the capacity and safety of international airports have to be faced. In order to increase airport capacities whilst at least maintaining safety levels, the knowledge of wake vortex behavior under varying meteorological conditions merits considerable significance. In principle, wake vortices descend below the glide path caused by mutual velocity induction. But under certain meteorological conditions, wake vortices may stall or rise again into the glide path corridor [8, 16, 30]. We show that, at least in the limits of 2D investigations, this hazardous situation actually may occur in strongly stratified atmospheres. Also, in the quite often prevailing moderately stratified environments, wake vortex behavior is considerably modified.

The climatology, based on nine years worth of data from nine different aerological stations in Germany [9], reports nocturnal inversions with potential temperature gradients of more than 1 °C/100 m in the lower troposphere in 59 % of all cases. In Munich 70 % inversions were found at midnight and at 9:00 LST 12 % were still persisting.

The impact of stable stratification on wake vortices has been a controversial discussion for years. Whereas some studies indicate that the vortices decelerate and stop their descent roughly after 1/4 of the oscillation period [7, 10, 11, 18, 21] or may even oscillate in a similar way as a displaced buoyant parcel of fluid [20], other analyses show that wake vortices may accelerate their descent due to baroclinic effects [2, 26]. Some works [4, 15, 22, 27] demonstrate that both events may occur in sequence. Consensus seems to emerge from recent 3D simulations [19, 24]. These corroborate our recent 3D simulation results which are part of ongoing work and will be published later: All 3D simulations show that during the early descent the wake vortices simultaneously decelerate and approach each other. This behavior is almost identically observed in 2D investigations and, furthermore, is also confirmed by experiments (see *figure 1*). The subsequent acceleration seen in 2D is widely damped in 3D by different instability mechanisms, whereas the type of instability depends on the state of turbulence in and around the vortex pairs.

The current work, although limited to two dimensions, is to deepen and to reach a consensus on the basic understanding of wake vortices in a stably stratified atmosphere. Among others, the physics of basic effects such as the deceleration and detrainment phenomena is investigated in detail. Please note, that the authors assume these early effects to be intrinsically two-dimensional. On the other hand, 3D studies are clearly needed to understand the subsequent trailing vortex decay.

2. Numerical model, initial conditions and normalized variables

The 2D code is based on a Boussinesq large-eddy simulation code which uses the classical Smagorinsky closure and was originally developed to simulate turbulence, i.e. fluctuations of velocity and temperature, under the influence of constant background shear and stratification [12]. The LES code was then tuned to model the dynamics of aircraft wakes and the associated exhaust distribution under cruising conditions [5]. In this context it proved its reliability, for it reproduced the typical wake structure and quantitative exhaust properties as observed in measurement campaigns [6].

For our purposes here, we chose a domain size of $L_x \times L_y \times L_z = 6 \times 384 \times 600\ \mathrm{m}^3$ with a uniform grid volume of $\Delta x \times \Delta y \times \Delta z = 1 \times 1 \times 1\ \mathrm{m}^3$. The flight direction is denoted by $-x$, the span by y and the height by z. Periodic boundary conditions are employed in all three directions. The influence of neighbouring wakes on the descent velocity, w, due to the boundary conditions, was reduced by choosing appropriate distances between the vortices and the domain boundaries and is proven to be less then 2.3 % for neutral stratification (see *figure 2*).

The wake vortices were initialized as superposition of two Lamb-Oseen vortices where the tangential velocity profile of one vortex is given by

$$v_t(r) = \frac{\Gamma_0}{2\pi r}\left(1 - \exp\frac{-r^2}{r_0^2}\right) \quad , \quad r_0 = \frac{r_c}{1.121} \quad , \quad (1)$$

with a core radius of $r_c = 4$ m. A root-circulation of $\Gamma_0 = 565\ \mathrm{m}^2/\mathrm{s}$ and a vortex spacing of $b_0 = 47$ m were employed to represent the B-747 aircraft with an elliptical wing loading. The mean temperature gradient of the atmosphere, $d\Theta/dz$, was constant in each calculation and the corresponding Brunt-Väisälä frequencies

$$N = \left(\frac{g}{\Theta_0}\frac{d\Theta}{dz}\right)^{1/2} \quad (2)$$

varied between 0 and 0.056/s ($0 \le d\Theta/dz \le 10$ K/100 m), i.e. between neutral and very stable stratification.

All results are presented in non-dimensionalized form. The characteristic scales are based on the initial vortex separation, b_0, and circulation, Γ_0, leading to the time scale

$$t' = \frac{2\pi {b_0}^2}{\Gamma_0} = \frac{b_0}{w_0} \, . \quad (3)$$

For the normalized time and Brunt-Väisälä frequency it follows $t^* = t/t'$ and $N^* = Nt'$, respectively. $1/N^*$ corresponds to the vortex Froude number.

3. General characteristics and phenomena

Figure 1 depicts the temporal development of the normalized descent height z/b_0, which was determined by searching the local pressure minima. For reference the linear descent for neutral stratification is included. In the most stable case, $N^* = 1.4$, the vortex behavior differs considerable from the other cases and, therefore, is discussed later in this section and partially omitted in the following sections. In the stable cases with $N^* \leq 1.0$ the descent is first decelerated and then progresses with an acceleration. The vortices reach their minimum descent velocity roughly at $t^* = 3$ (see *figure 2*) and, for $N^* = 1$, stall and even rise again a few meters to a height of approximately one initial vortex separation below flight level. Then they continue to descend and accelerate up to three times their initial speed.

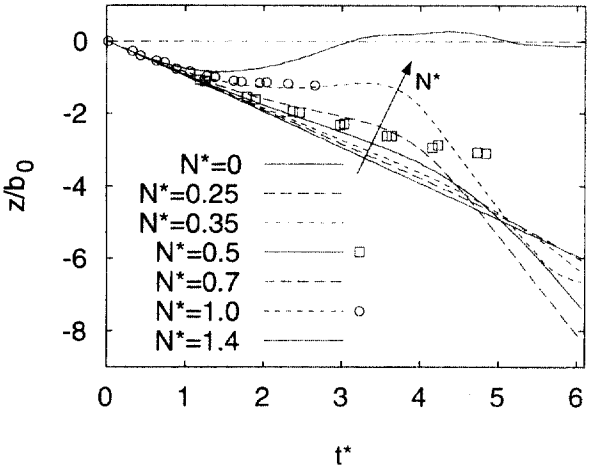

Figure 1. Normalized descent distance versus time for different stratifications. 2D-simulations (lines) and Sarpkaya's experimental data [21] (symbols).

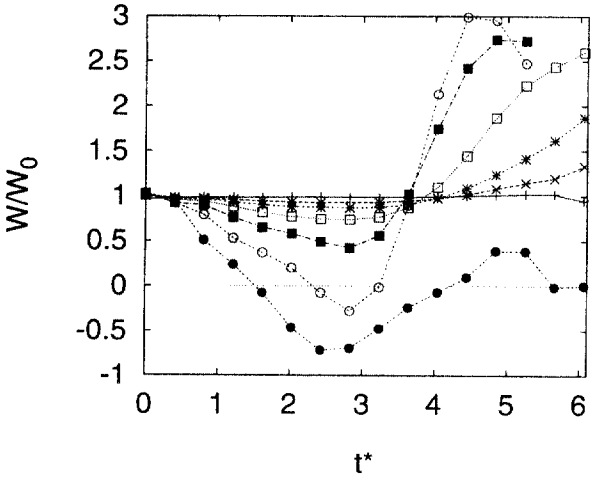

Figure 2. Simulated wake descent speed normalized by initial speed; legend see *figure 4*.

Please note that during the deceleration period the 2D results agree well with Sarpkaya's towing tank experiments [21] which are delineated with symbols in *figure 1*. The agreement clearly indicates that the physics of the early deceleration is intrinsically 2D. For the further evolution of the trailing vortices Sarpkaya states that the vortices were primarily destroyed by different 3D instability mechanisms which are, of course, excluded in the 2D simulations.

Figures 3 and *4* indicate that the vortex separation b/b_0 decreases drastically when $t^* > 2$ whereas the circulation Γ is largely conserved. (Note that Γ was integrated along the oval-like streamline which separates the fluid belonging to the wingtip vortices and the surrounding fluid. The lower values of Γ observed between $0.5 \leq t^* \leq 3.5$ result from the fact that at that time the oval encloses also counter-rotating vorticity, see below.) Our findings of a circulation remaining constant over a

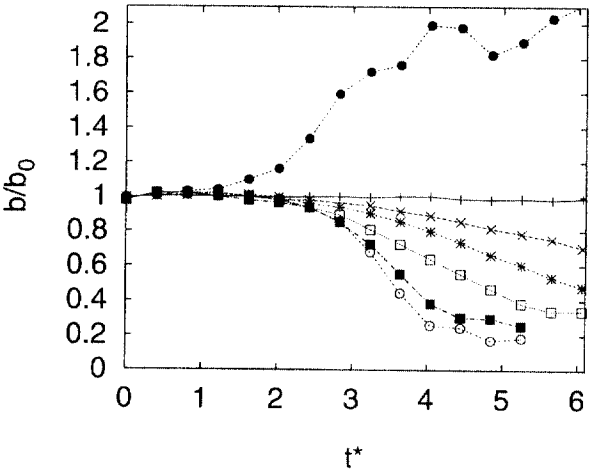

Figure 3. Simulated vortex spacing normalized by initial spacing; legend see *figure 4*.

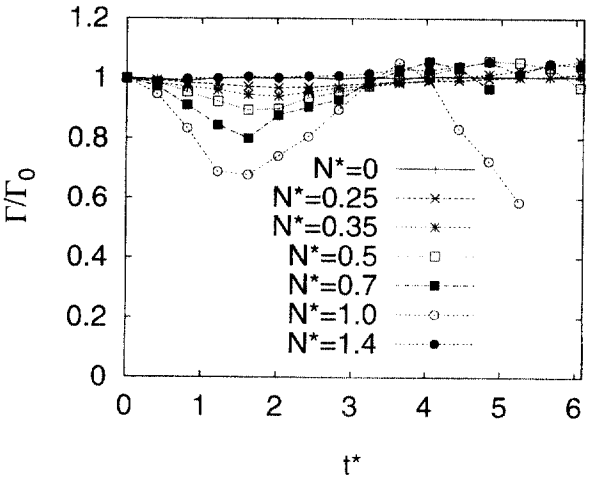

Figure 4. Simulated circulation normalized by initial circulation.

long period and dropping suddenly afterwards are in good agreement with measurements [8] but are in contrast to other work [7] which assumes a monotonous decrease of Γ. We notify that the approach of the vortices which de facto keep their initial circulation may explain the late acceleration of the vortex pair by the increased mutual velocity induction. It, however, leaves the early deceleration unexplained which may have led to some controversy in earlier works.

For $N^* = 1.4$ the vortices descend only about one vortex spacing, then rise again to remain, finally, on the flight level with unaltered circulation. The increasing vortex spacing, which reaches two times the initial spacing at $t^* = 6$, presumably, will impede rapid mutual destruction mechanisms such as the Crow instability. Here, the hazardous situation of two almost solitary and, thus, persistent vortices in the flight path may occur. 3D simulations will be needed to show whether this is likely to happen in reality. Since $N^* = 1$ constitutes the weakest stratification bearing slightly rising vortices it may be considered as a conservative threshold for this hazardous scenario.

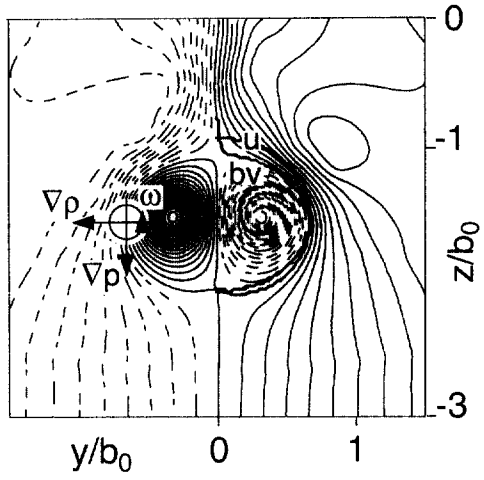

Figure 5. Sketch of vorticity production by the baroclinic torque. Integrated streamfunction contours are shown for $N^* = 1$ and $t^* = 3.1$. bv marks the actual and u the analytically achieved separating streamline.

4. Detailed analysis of phenomena

Basically, the oval around the vortex pair, which contains the primary vorticity and is termed the primary wake, descends and warms adiabatically in a stably stratified environment owing to compression. The evolving force does not simply decelerate the sinking motion of the oval as is often assumed when considering the oval as an ideal particle. But it creates secondary vorticity which has the opposite sign to the primary vorticity [26] in terms of the baroclinic torque according to

$$\frac{D\omega}{Dt} \sim \frac{1}{\rho^2} \nabla\rho \times \nabla p \,. \qquad (4)$$

This torque is effective when the gradients of density, ρ, and pressure, p, have perpendicular components as it is displayed schematically in a plot of isolines of the integrated streamfunction in *figure 5*.

The temperature contour plots in *figure 6* elucidate that the largest horizontal density gradients are not always found directly at the separating streamline as anticipated in previous work [11, 26]. In early stages ($t^* = 0.7$) when stratification effects still play a minor role, the vertical displacement of individual fluid particles is dominated by vortical advection resulting in the largest horizontal density gradients and, thus, in strongest baroclinical vorticity (BV) production 'inside' the oval. (This explains the transient decay of Γ as discussed above, see *figure 4*). Later ($t^* = 3.1$), the mean descent altitude causes the dominant density deviation from the ambient air.

Figure 7 displays contours of axial vorticity, ω_x, for $N^* = 1$. At $t^* = 3.1$ the vorticity of the primary vor-

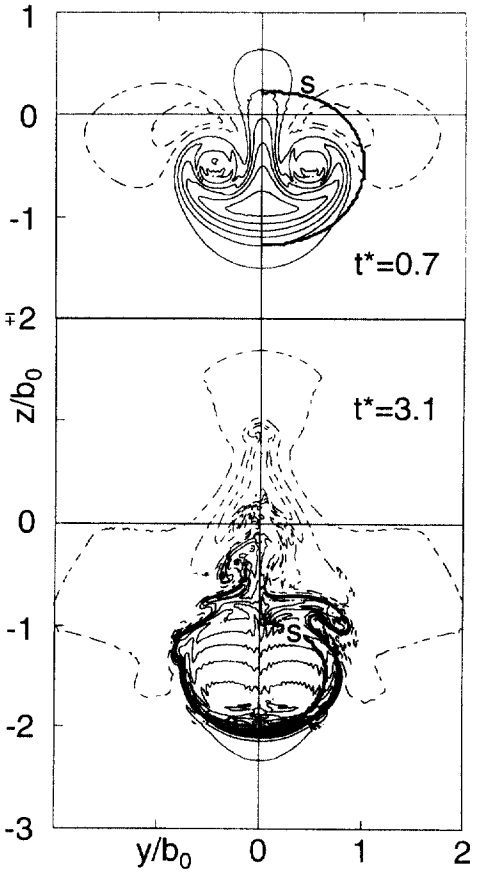

Figure 6. Temperature deviation for $N^* = 1$. Contour increments: 0.5 K, dashed lines mark negative values. Separating streamline is marked with *s*.

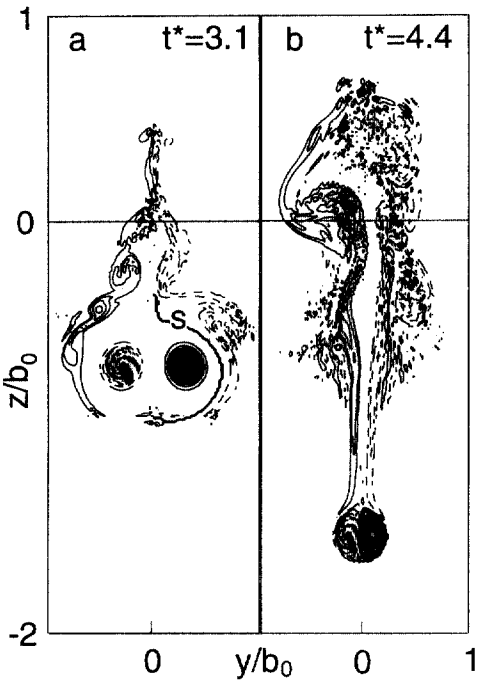

Figure 7. Axial vorticity ω_x at different times; $N^* = 1$. Contour increments: 0.25/s, dashed lines mark negative values. Separating streamline is marked with s.

tices still is isolated in the cores but almost entirely surrounded by BV. At the upper stagnation point the BV is completely left behind the oval and constitutes the secondary wake which extends from the primary wake to a height above the flight level. The temperature plot at $t^* = 3.1$ (*figure 6*) shows that the moving oval 'pushes' (below the lower stagnation point) and 'pulls' (above the upper stagnation point) ambient air downwards. Therefore, the steepest temperature gradients and, consequently, the maximum vorticity production occur just outside the separating streamline. This implies that the opposite vorticity is advected around the oval and is completely left behind the wake vortices. Hence, at this stage ($t^* = 3.1$) the question whether opposite vorticity can also be entrained into the oval is denied which is of great interest for the formation of instabilities and the decay of the vortices [26, 27].

The half rings of secondary vorticity surrounding the primary wake lead to a disturbance of the velocity field. *Figure 8* shows swirl velocity distributions $v_\theta(r)$ at three different times (these were derived by transforming the respective velocity fields into the tangential components of two axisymmetric vortices). The vortex at $t^* = 0.7$ is only little influenced by stratification which results in an induced descent velocity close to one at $r = b_{0.7}$. At $t^* = 2.3$, the swirl velocity decreases steeply in the vicinity of the separating streamline and $v_\theta(b_{2.3})$ almost vanishes. Hence, the primary wake stalls because the BV induces an upward motion inside the oval which compensates the downward motion of the primary vortex pair. However, such swirl velocity profiles are highly unstable according to the stability criterion defined by Rayleigh [17]. As a consequence, Taylor-Görtler instabilities evolve which can clearly be observed in the vorticity distribution displayed in *figure 7a*. Presumably, in the unstable region tiny roundoff errors in the initialization and discretization method are sufficient to raise the asymmetries observed in *figures 6* and *7*. But they do not generate a non-zero axial velocity component. At this stage, the secondary vorticity, which is still produced by the baroclinity, moves slowly upwards along the separating streamline. As we explain in the following section, the oval begins to lose mass (detrainment) in the vicinity of the upper stagnation point. To fulfil mass conservation constraints, the two main vortices have to strongly approach each other which, in turn, increases the induced descent speed (see *figures 2* and *3*) such that the vortices can eventually escape from their 'buoyancy trap' by quick downward motion (*figure 7b*). Note that the typical vortex profiles are established again during the fast descent (*figure 8*, $t^* = 4.4$). Hence, the main vortices have recovered from the 'buoyancy disease' but only to approach each other more and more which finally leads to their destruction by direct interaction as indicated by the sudden loss of their – so far conserved – circulation (*figure 4*). We remark here that the late stages are of academic interest because in 3D instability mechanisms would suppress the final acceleration.

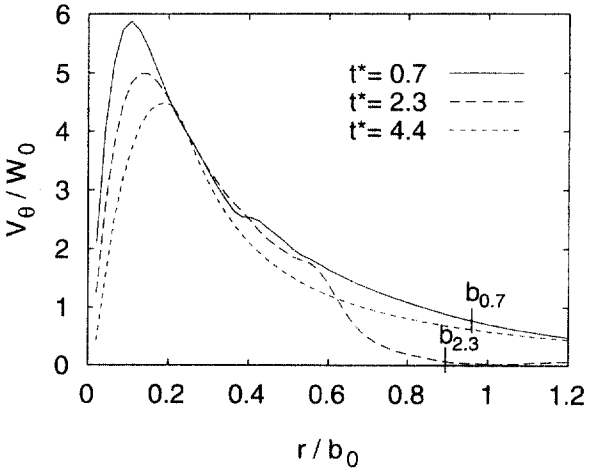

Figure 8. Swirl velocity profiles, $v_\theta(r)$, and respective vortex spacings at three different times; $N^* = 1$.

5. Kinematic description – deceleration and detrainment

One simple and evident explanation for the deceleration of the vortex pair is given by buoyancy. However, the inconsistence of the approaching vortices with

constant circulation and, nevertheless, decreasing descent speed remains unresolved. A more comprehensive view which also explains the detrainment phenomenon is achieved by considering the mutual velocity induction of primary and BV. Please note that this purely kinematic arguments provide a full reasoning of all effects since in the vorticity equations the influence of bouyancy exclusively is expressed by the baroclinic term.

Assuming the density discontinuity along the separating streamline, the BV production can readily be calculated according to equation (4) [26]. In (4) only the contributions of pressure gradients caused by the hydrostatic balance ($\partial p/\partial z = -\rho g$) have to be considered. Contributions from centrifugal forces vanish, since centrifugal pressure gradients and density gradients always are perpendicular to streamlines and, thus, parallel. For the axial vorticity component we obtain

$$\frac{D\omega_x}{Dt} = -\frac{g}{\rho}\frac{\partial \rho}{\partial y}. \tag{5}$$

The lateral density gradient over a layer of thickness δ can be expressed in terms of the Brunt-Väisälä frequency

$$\frac{\partial \rho}{\partial y} = \frac{\partial \rho}{\partial n}\sin\psi \equiv \frac{\Delta\rho}{\delta}\sin\psi = -\rho\frac{N^2 z}{g\,\delta}\sin\psi \tag{6}$$

where ψ is the angle made by gravity and the normal n to the separating streamline. The equation resulting from equations (5) and (6) can be non-dimensionalized using the time scale (3) and

$$\omega' = N^2\, t'\,\frac{z}{\delta} \tag{7}$$

which yields

$$\frac{D\omega_x^*}{Dt^*} = \sin\psi\,. \tag{8}$$

Note that equation (8) gives the BV production independent from the individual parameters. The produced BV accumulates during the advection of fluid particles along the separating streamline being weighted with the respective residence times. Hence, the strength of the vortex sheet increases from zero at the lower stagnation point to a maximum at the upper stagnation point, whereas the production rate is maximum at the height of the vortex cores and zero at the stagnation points.

Figure 9a depicts the velocity field which is induced by 164 point vortices situated along the separating streamline. The point vortices represent the BV for $N^* = 1.0$ during the stall in a descent height of $z/b_0 = -1.4$. Different descent heights and stratifications do not change the shape but only modify the magnitudes of the self–similar velocity field.

The upwards directed flowfield inside the oval together with the downwards velocities around the oval induce a reduction of the descent speed. The topology of the flowfield inside the oval is illustrated in a simple sketch (*figure 10*). Horizontally opposite point vortices 1, 2 induce vertical velocities which increase from below to above (see stronger vortices 3, 4). Vertically separated vortices 2, 3 induce upwards directed velocities with an additional horizontal component which manifests the approach of the vortex pair.

The superposition of the primary and the BV induced velocity fields is shown in *figure 9b*. Now, the calculation of the separating streamfunction *bv* leads to a basically modified shape: A part of the surrounding fluid is entrained below whereas a bigger part which used to belong to the oval is detrained above. The net fluxes reflect the detrainment mechanism. See also the shapes of the separating streamfunctions in the simulations (*figure 5*) which agree saliently well with the kinematic

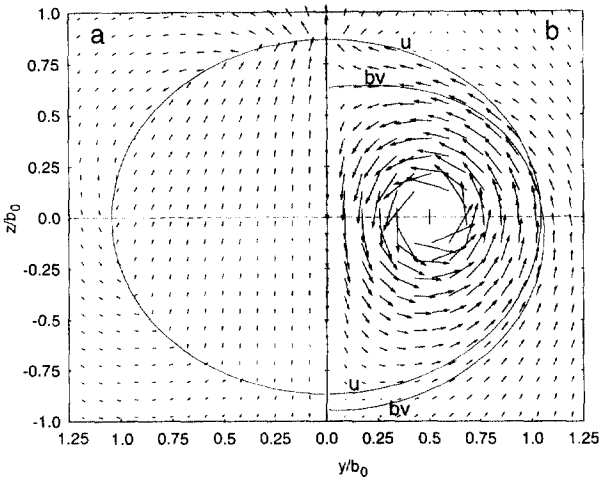

Figure 9. Velocity vectors from point vortex model. **a)** explicitly BV induced, **b)** superposition of BV induced and primary velocity field. *u* undisturbed and *bv* modified separating streamfunctions.

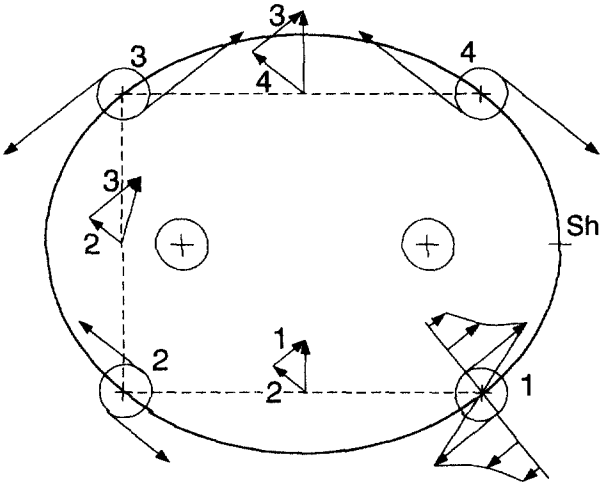

Figure 10. Sketch to illustrate the velocity field induced by BV. *Sh* denotes the position where the local shear–number is derived.

model, and, thus, 'prove' that the major effects are well demonstrated by the model.

The accelerated descent after $t^* = 3$ is also included in the kinematic approximation. For acceleration the vortex cores have to approach each other close enough to dominate the BV induced velocities.

Furthermore, the point vortex model may also be used to analyse buoyancy oscillations of spherical vortices which develop from any mass of buoyant fluid released in its environment [25, 28]. Various examples may be found in geophysical flows such as overshooting thunderstorms [23] or cloud turrets [3]. By dividing the oscillation into quarter periods, four different regimes can be identified which are delineated in *table I*. The sign of the temperature difference across the separating streamline determines the sign of the BV and, thus, together with the sign of the primary vorticity which changes during the transition from ascent to descent and vice versa, the ratio of the primary and BV. This leads, in turn, to entrainment of mass for positive vorticity ratios and to detrainment for negative vorticity ratios according to the above presented mechanisms. During one oscillation the regimes alternate such that after one oscillation the vortex ring has recovered to its initial mass.

Table I. Classification of the de- and entrainment behavior of an oscillating spherical vortex as function of the temperature of the vortex, T_{vor}, its environment, T_{amb}, and the signs of the primary, ω_{vor}, and baroclinic vorticity, ω_{bv}.

Descent	Ascent
$T_{vor} < T_{amb}$ $\omega_{vor}/\omega_{bv} > 0$ entrainment	$T_{vor} < T_{amb}$ $\omega_{vor}/\omega_{bv} < 0$ detrainment
$T_{vor} > T_{amb}$ $\omega_{vor}/\omega_{bv} < 0$ detrainment	$T_{vor} > T_{amb}$ $\omega_{vor}/\omega_{bv} > 0$ entrainment

6. Deceleration or acceleration – the local shearnumber

By relating the BV produced shear S_B to the shear of one primary vortex S_V a local shear–number $Sh = S_B/S_V$ can be deduced which describes the instantaneous tendency of wake vortices to accelerate or to decelerate. The local shear–number is derived at the vertical flanks of the oval (see Sh in *figure 10*). This position is considered to be representative for the whole oval, because here the accumulated BV amounts to 50 % of its maximum value.

The BV produced at the flanks in a layer of thickness δ can be calculated numerically from equation (8) and amounts to $\omega_x^* = 0.6775$. Using (7) and (3) we obtain

$$\omega_x = 0.6775\, N^2 \frac{2\pi b^2}{\Gamma} \frac{z}{\delta}. \qquad (9)$$

$\omega_x = \dfrac{\partial w}{\partial y} - \dfrac{\partial v}{\partial z}$ corresponds directly to $S_B = \partial w/\partial y$ at the vertical flanks, because $\partial v/\partial z = 0$ for symmetry reasons. For the primary vorticity the shear of a Rankine vortex, at a radius corresponding to the distance of the vortex core to the vertical flank of $0.545\,b$, is used, which amounts to $S_V = 3.37\Gamma/(\pi b^2)$. This leads to the local shear number

$$Sh = \frac{S_B}{S_V} = 3.97\, z\, N^2\, b^4/(\Gamma^2 \delta). \qquad (10)$$

Assuming one unit thickness for δ, *figure 11* characterizes well the regimes of deceleration for $Sh > 1$ (BV dominates) and acceleration for $Sh < 1$ (primary induced velocities dominate).

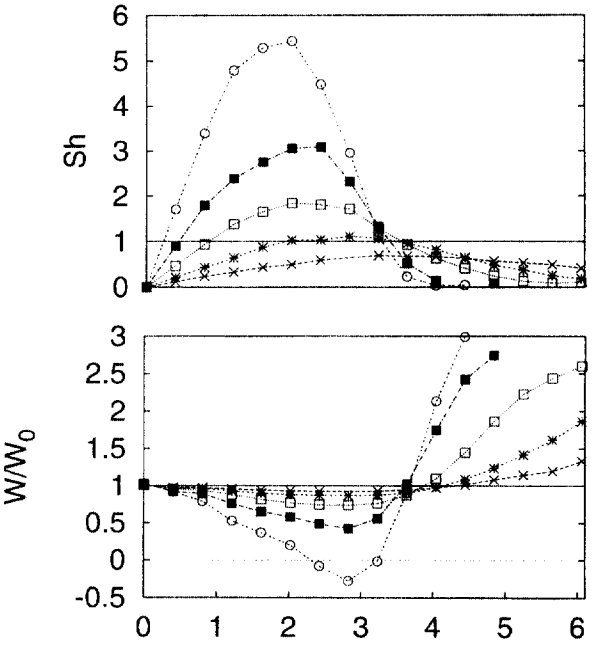

Figure 11. Local shear number, above, describing the state of acceleration or deceleration, below. Legend see *figure 4*.

7. Integral description - the impulse

After the analysis of the impact of local effects upon the wake flow behavior, this section deals with an integral description of the generic phenomena in terms of impulse. Such approaches are needed as part of wake vortex prediction algorithms [1, 7, 13, 26, 27] which are designed to predict the lifespan of particular wake vortices as a function of aircraft parameters and meteorological conditions. Approaches based on impulse are

thought to be more general because they do not rely on assumptions of specific tangential velocity profiles, as do approaches based on the kinetic energy. Nevertheless, the contribution of the rotational motion to the development of the impulse is not clear and will, therefore, be addressed in this section.

Figure 12 displays various formulations of the impulse per unit length normalized by its initial value, $I_0 = \rho b_0 \Gamma_0$, as function of the oscillation period. Three different approaches, according to equations (11), (14), and (15) are employed, where the curves with symbols denote evaluations of our simulations following equations (11) and (15). Please note that in spite of the differing characteristics at varying stratification levels (see *figures 1* to *3*), the respective graphs clearly coincide with both methods.

Full symbols represent the impulse determined for the oval. It is calculated using

$$I_{\text{oval}} = \rho A w + 0.55\, \rho b \Gamma . \tag{11}$$

Here, A denotes the area of the oval; the vertical coordinate z and hence I are defined positive downwards for convenience in this subsection. The first term represents the translational momentum of the descending oval and the second term the contribution of the rotation to the oval's impulse (in a manner similar to the concepts of the reduced mass of a rolling wheel, which is used to calculate its resistance to acceleration). The factor 0.55 may be derived as follows: By considering the differential equation for the undamped oscillation of a vortex pair confined in an oval with the area A [7]

$$\frac{d^2 z}{dt^2} + \underbrace{\frac{\rho A}{2\pi \rho b^2}}_{0.45} N^2 z = 0 \tag{12}$$

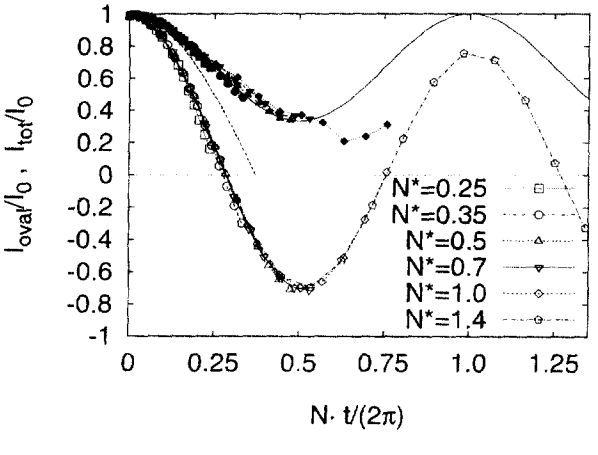

Figure 12. Normalized impulses versus the oscillation period. Impulses integrated over the oval of the primary wake (I_{oval}/I_0, full symbols; fit according to equation (13), solid line), over the area of the total wake (I_{tot}/I_0, open symbols), and according to equation (14) (dashed line).

a factor 0.45 arises in the linear term compared to the equivalent term in the equations for a non-rotating equal-area fluid particle. 1/0.45 represents the ratio of the reduced mass to the oval's mass. Hence, the contribution of the rotational motion is determined as $1 - 0.45 = 0.55$.

Figure 12 shows further that the impulse of the oval may be fitted (solid line) by

$$\frac{I_{\text{oval}}}{I_0} = \frac{1}{3} \cos Nt + \frac{2}{3} . \tag{13}$$

Please note the independence of N. Even the change of sign of the descent speed and, thus, the translational momentum for $N^* = 1$ in the interval $0.38 \leq Nt/(2\pi) \leq 0.51$ does not cause deviations. Obviously, the impulse is *stored* in the rotational motion. Likewise, the subsequent acceleration does not result in an increase of I_{oval} because it is compensated by the decrease of A.

In Greene's well-known wake vortex prediction approach [7], the influence of stable stratification is modeled in terms of impulse per unit length which is reduced by the buoyancy force

$$\frac{dI}{dt} = F_b = -\rho A N^2 z . \tag{14}$$

The wake is assumed to decay within a quarter of the oscillation period when the impulse of the oval reaches zero (see *figure 12*, dashed line). The oscillation period, however, is augmented for a factor of $1/\sqrt{0.45} \approx 1.5$ by taking into account the contribution of the rotation to the impulse in terms of reduced mass (see above). Nevertheless, our calculations show that I_{oval} has merely reduced to 0.44 I_0 at one quarter of the modified oscillation period. We argue that the assumption of a constant vortex spacing is responsable for the deviation.

In contrast to that, the development of the impulse for the whole system, I_{tot}, including both primary and secondary wake, excellently confirms the Brunt-Väisälä theory, see open symbols in *figure 12*. This impulse is integrated according to [14]

$$I_{\text{tot}} = -\iint \rho\, \omega_x\, y\, dy\, dz . \tag{15}$$

To achieve this result the secondary wake must be considered, i.e. the boundaries for integration must be well defined.

A more refined interpretation of the underlying mechanisms can be given by considering the bouyancy force, F_b (equation 14), which acts on the oval. *Figure 13* depicts the temporal evolution of the integrated F_b (open symbols) and the corresponding development of the idealized buoyant particle (solid line). The interesting fact that both coincide at least 0.25 periods means that the product of the decreasing size of the oval, A, and the increasing vertical displacement, z, of the primary wake equals the corresponding product for a constant A and the sinusoidal oscillation of z of an idea-

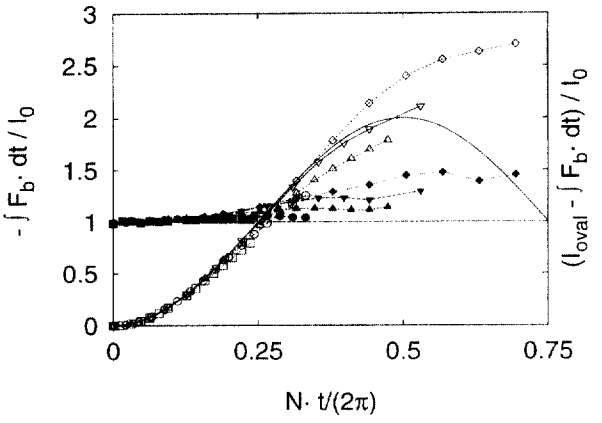

Figure 13. Integrated normalized bouyancy force of the oval (open symbols) and an idealized particle (solid line), left ordinate. Normalized difference between impulse and integrated bouyancy force (full symbols), right ordinate.

lized particle. Therefore, a relation between the descent height and the size of the oval - and, thus, implicitly of the vortex spacing - can be deduced from

$$z(t)A(t) = \frac{A_0 w_0}{N} \sin Nt \,. \qquad (16)$$

According to equation (14), the difference between the impulse and the time integral of F_b must be I_0. The graphs (full symbols) in *figure 13* show a growing contribution to the impulse of the oval. This increase again is caused by the neglect of the secondary wake. *Figure 5* elucidates that during the stagnation of the oval the surrounding fluid is *blown* upwards. Hence, the primary and secondary vortices may be considered as a two-mass system in which the primary wake balances its impulse by accelerating the secondary wake upwards.

8. Conclusions

We have performed 2D simulations of wake vortices in stable stratification evaluating the temporal development of characteristic quantities such as descent height and speed, vortex spacing and circulation. Together with instantaneous flow pictures in terms of streamlines, temperature and vorticity fields, these data give a survey and detailed insight in 2D wake vortex physics. Considering additionally the kinematic model presented and the derived local shear–number the results clearly suggest that the sequential deceleration and acceleration as well as the detrainment phenomenon are dominantly caused by mutual velocity induction of the primary vorticity caused by the aircraft and the secondary vorticity produced by baroclinity.

The evaluations of the impulse of the wake oval itself and the total wake, including primary and secondary produced vorticity, demonstrate that the oscillation assumed in theory is executed by the whole system and not by the oval alone. The vortex oval performs complex displacement patterns which, at a first glance, seem to contradict the laws of conservation.

The similarity of the phenomena reported here (with a constant temperature gradient in the entire domain) and by Pavlenko [15] suggest that the interpretations also can hold for the immersion of wake vortices into stable layers. We argue that a gradually increasing temperature difference (as here) or a sudden jump in the temperature difference (as observed during the penetration of the vortices into an inversion layer) only result in second-order differences but will lead to the same fate in principal for an aircraft wake.

Our findings complement recent findings of the 3D trailing vortex behavior in stable stratification by elucidating intrinsically 2D elements of the complex wake vortex physics. Thus, they may help to bring together contrary results and assumptions in the analysis and modeling of vortices in stably stratified environments.

Acknowledgements

This work was supported by the European Commission in the frame of the Brite/EuRam project WAVENC (No. BE97-4112).

References

[1] Corjon A., Poinsot T., Vortex Model to Define Safe Aircraft Separation Distances, J. Aircraft 33 (1996) 547–553.

[2] Crow S.C., Motion of a vortex pair in a stably stratified fluid, Poseidon Research Rep. 1, Santa Monica, CA, (1974).

[3] Fujita T.T., Overshooting Tops observed from ATS and Learjet, SMRP Research Paper 117, University of Chicago.

[4] Garten J.F., Arendt S., Fritts D.C., Werne J., Dynamics of counter-rotating vortex pairs in stratified and sheared environments, J. Fluid Mech. 361 (1998) 189–236.

[5] Gerz T., Ehret T., Wingtip vortices and exhaust jets during the jet regime of aircraft wakes, Aerospace Sci. Techn. 1 (1997) 463–474.

[6] Gerz T., Holzäpfel F., Wingtip Vortices, Turbulence and the Distribution of Emissions, AIAA J., in press.

[7] Greene G.C., An Approximate Model of Vortex Decay in the Atmosphere, J. Aircraft 23 (1986) 566–573.

[8] Greenwood J.S., Vaughan J.M., Measurements of Aircraft Wake Vortices at Heathrow by Laser Doppler Velocimetry, Air Traffic Control Quarterly 6 (1998) 179–203.

[9] Gutsche A., Inversionen in der unteren Troposphäre nach Radiosondenaufstiegen in der Bundesrepublik Deutschland, Deutscher Wetterdienst, Zentralamt Abteilung Klimatologie, (1978).

[10] Hecht A.M., Bilanin A.J., Hirsh J.E., Turbulent Trailing Vortices in Stratified Fluids, AIAA J. 19 (1981) 691–698.

[11] Hill F.M., A numerical study of the descent of a vortex pair in a stably stratified atmosphere, J. Fluid Mech. 71 (1975) 1–13.

[12] Kaltenbach H.-J., Gerz T., Schumann U., Large-eddy simulation of homogeneous turbulence and diffusion in stably stratified shear flow, J. Fluid Mech. 280 (1994) 1–40.

[13] Kantha L.H., Empirical Model of Transport and Decay of Aircraft Wake Vortices, J. Aircraft 35 (1998) 649–653.

[14] Lamb Sir H., in: Hydrodynamics, Dover publ., 1945, 214–216.

[15] Pavlenko A.A., Influence of the Calm Atmosphere Stratification on the Evolution of the Vortex Behind an Aircraft, ISTC Moscow, Annual Report, Project No. 201–95 (1996) 33–40.

[16] Proctor F.H., Hinton D.A., Han J., Schowalter D.G., Lin Y.-L., Two Dimensional Wake Vortex Simulations in the Atmosphere: Preliminary Sensitivity Studies, 35th Aerospace Sciences Meeting & Exhibit, Reno, NV, AIAA 97-0056 (1997).

[17] Rayleigh Lord O.M., On the Dynamics of Revolving Fluids, P. Roy. Soc. Lond. A Mat. 93 (1917) 148–154.

[18] Robins R.E., Delisi D.P., Numerical Study of Vertical Shear and Stratification Effects on the Evolution of a Vortex Pair, AIAA J. 28 (1990) 661–669.

[19] Robins R.E., Delisi D.P., Numerical Simulation of Three-Dimensional Trailing Vortex Evolution in Stratified Fluid, AIAA J. 3 (1998) 981–985.

[20] Saffman P.G., The Motion of a Vortex Pair in a Stratified Atmosphere, SIAM LI (1972) 107–119.

[21] Sarpkaya T., Trailing vortices in homogeneous and density-stratified media, J. Fluid Mech. 136 (1983) 85–109.

[22] Schilling V., Siano S., Etling D., Dispersion of aircraft emissions due to wake vortices in stratified shear flows: A two-dimensional numerical study, J. Geophys. Res. 101 (1996) 20965–20974.

[23] Schlesinger R.E., Overshooting Thunderstorm Cloud Top Dynamics as Approximated by a Linear Lagrangian Parcel Model with Exact Solutions, J. Atmos. Sci. 47 (1990) 988–998.

[24] Schowalter D.G., DeCroix D.S., Switzer G.F., Lin Y.–L., Arya S.P., Toward Three-Dimensional Modeling of a Wake Vortex Pair in the Turbulent Planetary Boundary Layer, 35th Aerospace Sciences Meeting & Exhibit, Reno, NV, AIAA 97-0058 (1997).

[25] Scorer R.S., Experiments on convection of isolated masses of buoyant fluid, J. Fluid Mech. 2 (1957) 583–594.

[26] Scorer R.S., Davenport L.J., Contrails and aircraft downwash, J. Fluid Mech. 43 (1970) 451–464.

[27] Spalart P.R., On the motion of laminar wing wakes in a stratified fluid, J. Fluid Mech. 327 (1996) 139–160.

[28] Turner J.S., Buoyant vortex rings, P. Roy. Soc. Lond. A Mat. 239 (1917) 61.

[29] Urbatzka E., Wilken D., Estimating Runway Capacities of German Airports, Transportation Planning and Technology 20 (1997) 103–129.

[30] Zak J.A., Rodgers Jr. W.G., Documentation of Atmospheric Conditions During Observed Rising Aircraft Wakes, NASA Contractor Rep. 4767 (1997).